УДК 536.2.004.414.23:532.5.004.414.23

Влияние продольного расстояния на гидродинамические характеристики и теплообмен при поперечном обтекании шахматного пучка труб каплевидной формы

Дееб Равад

Национальный исследовательский университет «МЭИ»
Россия, Москва, 111250, Красноказарменная, 14
e.rawad.deeb@yandex.com

Аннотация

Численным методом было проведено исследование влияния продольного шага на характеристики потока и теплообмен при поперечном обтекании шахматного пучка труб каплевидной формы при нулевом угле атаки. Работа выполнена для диапазона чисел Рейнольдса $\mathrm{Re} = 3.18 \times 10^3 \div 3.25 \times 10^4$ и для продольных шагов $S_L = 37$ и 46.25 мм. Разработана математическая модель и алгоритм расчета теплообмена и гидродинамики пучка каплевидных труб с помощью программного пакета ANSYS FLUENT с учетом напряженно-деформированного состояния труб. Представлены корреляции, позволяющие определить средние число Нуссельта Nu и коэффициент трения f, для рассматриваемого пучка труб, в зависимости от Re и S_L. Результаты настоящего исследования показывают, что пучок труб с продольным шагом 46.25 мм имеет более интенсивный теплообмен с меньшим гидродинамическим сопротивлением по сравнению с пучком с шагом 37 мм. Было найдено, что тепло-гидравлические характеристики пучка каплевидных труб примерно в $18.1 \div 43.7$ раза больше, чем пучка труб круглого сечения.

Ключевые слова: каплевидные трубы, теплообмен, коэффициент трения, продольный шаг, численное исследование.
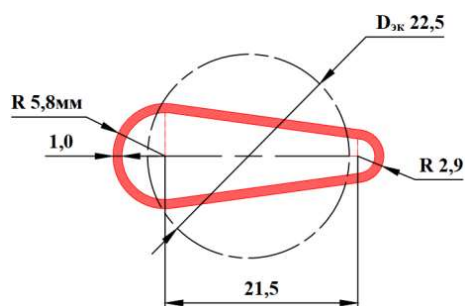
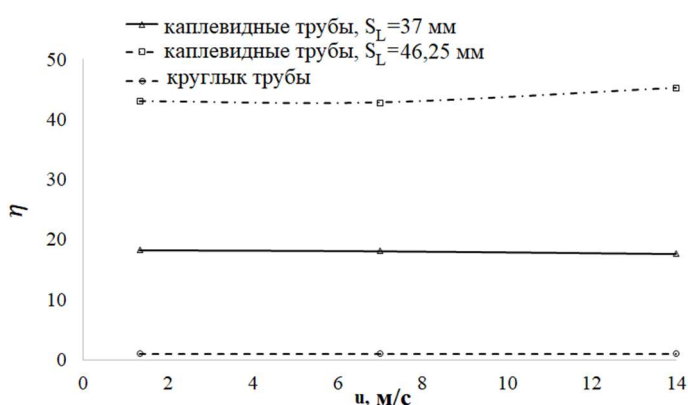Рис. 1. Поперечное сечение каплевидной трубы без нагрузки

Рис. 2. Тепло-гидравлические характеристики пучка круглых и каплевидных труб

Effect of Longitudinal Spacing on the Flow Characteristics and Heat Transfer for Staggered Drop-Shaped Tubes Bundle in Cross-Flow

Deeb Rawad

National Research University (Moscow Power Engineering Institute),
Moscow, 111250, Russia

e.rawad.deeb@yandex.com

Abstract

A numerical study has been conducted to investigate the effect of the longitudinal spacing on the flow and heat transfer characteristics for a staggered drop-shaped tubes bundle at zero angle of attack in crossflow. The study is performed for the Reynolds number $\mathrm{Re} = 3.18 \times 10^3 \div 3.25 \times 10^4$, while the longitudinal spacing S_L is 37 and 46.25 mm. A mathematical model and calculation algorithm using software package ANSYS FLUENT have been developed for numerical evaluation of heat transfer and flow field of a bundle of drop-shaped tubes, taking into account the strain caused by different pressures inside and outside the tubes. Correlations of the average Nusselt number Nu_{av} and a friction factor f in terms of Re and S_L for the studied bundle was presented. The results of the present study indicate that a drop-shaped tubes bundle with $S_L = 46.25$ mm has more intense heat transfer with less hydrodynamic resistance as compared to a bundle with $S_L = 37$ mm. The thermal–hydraulic performance of the studied drop-shaped tube bundle is about $18.1 \div 43.7$ times greater than the circular one.

Keywords: drop-shaped tube, heat transfer, friction factor, longitudinal spacing, numerical investigation.

1.   Introduction

Circular tubes bundles are widely used in heat exchange equipment because of the ease of production and its capability of withstanding a high pressure. In contrast to the circular tubes which cause severe separation and a large vortex zone to produce high pressure drops, non-circular tubes of streamlined shapes offer very low hydraulic resistance. The tubes bundles have numerous applications in the field of the process cooling towers, automotive radiators, heat exchanger tubes, chimney stacks, and gas pipelines. The arrangement of the tubes with respect to the free stream flow direction can be classified as in-line and staggered. Staggered tube bundle is easy to manufacture, it has a high heat transfer rate, satisfactory pressure drops. There are numerous studies that take into account the effect of the geometry and arrangement of the tubes in the bundle on the performance of heat exchangers. Staggered tubes bundles provide better thermal performance as compared to in-line one with slightly higher pressure drop [1, 2]. Nishimura et al. [3] investigated flow and mass transfer characteristics in a staggered and in-line arrangement. Reynolds numbers were ranged from 50 to 1000. They found that with increasing Reynolds number, the onset location of vortex shedding moves upstream, and the upstream development of flow transition are much faster for the tubes with staggered arrangement by comparing with the in-line arrangement.

In recent decades, several studies of non-circular tubes have been considered as heat transfer elements in cross-flow heat exchangers. Lavasani [4] experimentally investigated the flow around cam shaped tube bank with inline arrangement for both longitudinal pitch ratios 1.5 and 2. It was noted that by increasing longitudinal pitch ratios from 1.5 to 2, heat transfer increases about $7 \div 14$ %.

Furthermore, friction factor of cam shaped tube bank is approximately 95 % lower than circular tube bank. Toolthaisong and Kasayapanand [5] experimentally investigated the effect of the attack angles on heat transfer and the pressure drop characteristics in the air side of un-fined cross flow heat exchangers with the flat tubes have different aspect ratio. They found that the best thermal-hydraulic performance occurred at the 0 of attack angles. Merker and Hanke [6] experimentally investigated heat transfer and pressure drop of the cross-flow on the shell-side of staggered oval-shaped tubes bundle, having different transversal and longitudinal pitches. They found that the pressure drop decreases with increasing relative transversal pitch and Reynolds number. Horvat et al [7] numerically compared the heat transfer conditions for the tube bundle in cross flow for different tube shapes as cylindrical, ellipsoidal, and wing-shaped. The pitch to the diameter ratio in the staggered arrangement was from 1.125 to 2.0. Their results showed that drag coefficient is lower for ellipsoidal and wing-shaped tubes than that for the cylindrical tubes. However, drag coefficient decrease with increasing the Reynolds number. The effects of angles of attack on the heat transfer characteristics and the drag coefficient for staggered drop-shaped tubes were experimentally and numerically investigated by Sayed Ahmed et al. [8, 9]. They found that the average Nu values at zero angle of attack ($\theta=0$) was higher by about 76 % compared to elliptical tubes bundle with the same heat transfer surface. In addition, the lowest values of pressure drop were achieved at zero angle for all values of Reynolds numbers.

Correlation to predict friction factor and heat transfer coefficients have been attempted by various investigators. These correlations offer a means of assessing the heat transfer and pressure losses quickly without the need for expensive computational methods. Zhukauskas and Ulinskas [10, 11] suggested correlations for heat transfer and pressure drop for staggered and in-line of circular tubes bundles, each of 1.25×1.25, 1.50×1.50 and 2.0×2.0 pitch ratios, of 30 mm diameter tubes in cross-flows. They suggested an efficiency factor for the evaluation of heat transfer surfaces efficiency to improve heat exchangers constructions. A general equation for friction factor, based on tube gap spacing and gap velocity was developed by Chilton and Generaux [12]. Grimison [13] correlated the experimental data of Huge [14] and Pierson [15] for tube banks having 10 or more rows of tubes in the flow direction and for the various values of Re, subject to the transverse and longitudinal spacings. Gunter and Shaw [16] proposed a friction factor correlation for bare tubes using an equivalent hydraulic diameter as well as transverse and longitudinal pitch to diameter ratios. Friction factors of diameters between 0.5 and 127 mm were included, and transverse and longitudinal spacings were varied from 1.25 to 5 diameters.

In addition, many researchers have contributed their study to the investigation of the effect of longitudinal spacing on heat transfer and flow characteristics. Kim [17] studied the effect of the longitudinal spacing on flow characteristics for the in-line tube bundle in cross-flow using the CFD code FLUENT. Results indicated that the effect of the longitudinal spacing should be considered when the compact heat exchange is designed. Mittal et al. [18], numerically, investigated the flows past a pair of cylinders in staggered and in-line arrangements for different longitudinal spacing using a stabilized finite element method. They concluded that with increasing the longitudinal spacing, the flow at Re = 100 showed unsteady behavior. Numerical simulation is carried out by Roychowdhury et al. [19] to investigate the effect of spacing on flow and heat transfer over staggered tube bundles. They observed that both the Reynolds number and tube spacing influence the vortex formation. As the tube spacing increases, the size and length of eddies increase. For sufficiently small spacing and for all values of Reynolds number, eddy completely suppressed. Nishiyama et al. [20] studied the effects of longitudinal spacing on the drag coefficient for the staggered tubes bundle. They concluded that to achieve compactness of the system and minimize the drag coefficient, the longitudinal spacing should be arranged as small as possible. Mahir and Altac [21], numerically, investigated unsteady laminar convective heat transfer from two cylinders in a tandem arrangement. Reynolds number was ranged from 100 to 200 and the ratio L/D were varied from 2 to 10. They found that the mean Nusselt number of the upstream cylinder approaches to that of single cylinder for $L/D \geq 4$. Deng et al. [22] studied three-dimensional transition in the wake of flow passing around two circular cylinders in a

tandem arrangement. Their investigation covered a range of $220 \leq \text{Re} \leq 270$ and $1.5 \leq L/D \leq 8$. Results show that at $\text{Re} = 220$ and for $L/D \leq 3.5$, the flow can be treated as a two-dimensional system, but this treatment will be invalid for $L/D \geq 4$. Zdravistch et al. [23] proposed a numerical method, using the Reynolds-averaged Navier–Stokes equations (RANS), for calculating the tubes bundle heat transfer for laminar and turbulent flows. They found that a two-dimensional numerical simulation of the tubes bundle problem produces good results consistent with the three-dimensional one.

Computational Fluid Dynamics (CFD) emerged as a reliable and cost-effective method to simulate complex turbulent flows. Several researchers have identified the best combination of modeling and numerical method, in terms of accuracy and computational cost. Robertson et al. [24] investigated the physical mechanisms leading to vortex breakdown in high angle of attack flows over delta wing geometries using the open-source CFD solver OpenFOAM in parallel with the CFD solver ANSYS FLUENT. They concluded that a second-order upwind scheme with limiters is the most stable, has the smallest computational cost, and provides the most accurate results for RANS simulations. Dehkordi and Jafari [25] numerically simulated the 2-D unsteady viscous flow around two circular cylinders in a tandem arrangement in order to study the characteristics of the flow. Their results indicate that the extended $k - \varepsilon$ and the Re-Normalization Group (RNG) $k - \varepsilon$ models offer more accurate results than the standard $k - \varepsilon$ model. Priyank et al. [26] used FLUENT Software to analyze for predicting fluid flow and heat transfer characteristics over a staggered tube bundle heat exchanger with different tube bundles. They reported that CFD is the best tool for predicting fluid flow and heat transfer characteristics prior to the physical setup of the experiments. RNG $k - \varepsilon$ turbulence model improves the ability to model highly strained flows, vortices, separation, and recirculation of the fluid. The RNG $k - \varepsilon$ model showed an excellent agreement between numerical and experimental results [27, 28, 29].

The subject of this study is to evaluate the longitudinal spacing on heat transfer and flow behavior around the staggered drop-shaped tubes bundle in cross-flow. The deformation caused by pressure drop inside and outside the tubes was taken into account. Numerical simulations have been conducted using the software package ANSYS FLUENT to provide a detailed study of heat transfer and friction factor affecting the thermal-hydraulic performance of the studied bundle. Correlations of the Nu_{av} and f for the studied bundle was obtained for $\text{Re} = 3.18 \times 10^3 \div 3.25 \times 10^4$ and for $S_L = 37 \div 46.25$ mm.

2.   Numerical investigation

2.1.   Geometrical model

Using ANSYS, a numerical study of heat transfer and hydrodynamics of a bundle of 45 drop-shaped tubes (Fig. 1) is carried out. Drop-shaped tubes are located in a square cross-section channel, a side of the square cross-section is 305 mm with the following dimensions: the large radius is 5.8 mm, the small radius is 2.9 mm, the equivalent diameter D_{eq} is 22.5 mm (Fig. 2). The transversal and longitudinal spacing in the range of $S_T = 37$ mm and $S_L = 37 \div 46.25$ mm, respectively.

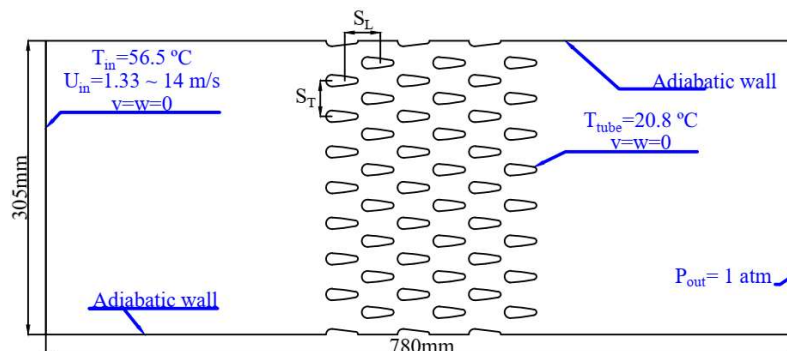
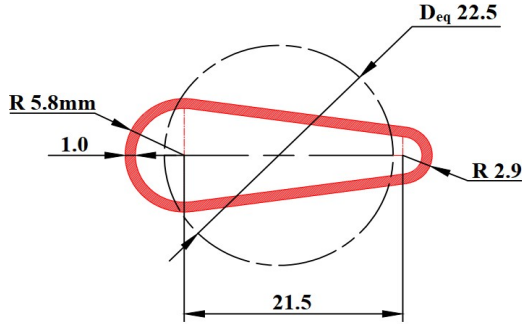Fig. 1. Schematic plane of the test section with boundary conditions
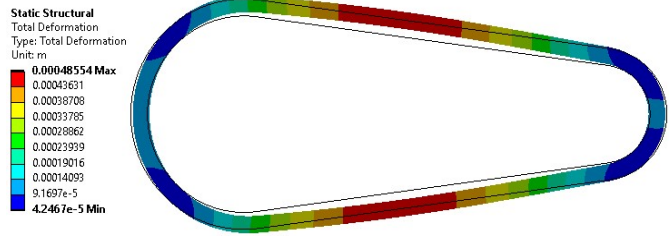
Fig. 2. Drop-shaped tube cross-section dimensions

Fig. 3. Stress-strain state

2.1. Problem description and boundary conditions

The forced convection problem has been solved using ANSYS FLUENT [30] in a two-dimensional stationary formulation assuming a viscous incompressible flow with constant thermophysical properties, taking into account the possibility of turbulence generation. The effect of heat exchange by radiation are neglected. The system of differential conservation equations includes the continuity equation, two momentum equations, and the energy equation

$$\frac{\partial u}{\partial x} + \frac{\partial v}{\partial y} = 0,$$ (1)

$$u\frac{\partial u}{\partial x} + v\frac{\partial u}{\partial y} = -\frac{1}{\rho}\frac{\partial p}{\partial x} + \upsilon\left(\frac{\partial^2 u}{\partial x^2} + \frac{\partial^2 u}{\partial y^2}\right),$$

$$u\frac{\partial v}{\partial x} + v\frac{\partial v}{\partial y} = -\frac{1}{\rho}\frac{\partial p}{\partial y} + \upsilon\left(\frac{\partial^2 v}{\partial x^2} + \frac{\partial^2 v}{\partial y^2}\right),$$ (2)

$$u\frac{\partial T}{\partial x} + v\frac{\partial T}{\partial y} = a\left(\frac{\partial^2 T}{\partial x^2} + \frac{\partial^2 T}{\partial y^2}\right)$$ (3)

where, u is the x-component of the air velocity; v is the y-component of the air velocity; ρ is the air density; p is the air pressure; υ is the air kinematic viscosity; a is the thermal diffusivity; T is the air temperature.

The modeling process is carried out in two stages. Firstly, the stress-strain state modeling has been performed using ANSYS Static Structural, the deformations caused by different pressures inside (14 bar) and outside the tubes (1 bar) have been determined. Figure 3 illustrates the cross section of the drop-shaped tube after deformation.

In the second stage, the turbulence is modeled by RNG $k-\varepsilon$ model with the "Enhanced wall Treatment" function]27, 30[. The turbulence of flow is expressed in turbulence kinetic energy (k) and dissipation rate (ε), using the following equations:

$$\frac{\partial}{\partial t}(\rho k) + \frac{\partial}{\partial x_i}(\rho k u_i) = \frac{\partial}{\partial x_j}\left(\alpha_k \mu_{eff}\frac{\partial k}{\partial x_i}\right) + G_k + G_b - \rho\varepsilon - Y_M + S_k,$$ (4)

$$\frac{\partial}{\partial t}(\rho\varepsilon) + \frac{\partial}{\partial x_i}(\rho\varepsilon u_i) = \frac{\partial}{\partial x_j}\left(\alpha_\varepsilon \mu_{eff}\frac{\partial\varepsilon}{\partial x_i}\right) + C_{1\varepsilon}\frac{\varepsilon}{k}(G_k + C_{3\varepsilon}G_b) - C_{2\varepsilon}\rho\frac{\varepsilon^2}{k} - R_\varepsilon + S_\varepsilon$$ (5)

In the above equations, μ_{eff} is the effective viscosity (the sum of molecular viscosity μ and turbulent viscosity μ_t); G_k, G_b represents the generation of turbulent kinetic energy due to mean velocity gradients and buoyancy, respectively; Y_M indicates fluctuating dilatation incompressible turbulence

to the overall dissipation rate; α_k and α_ε are the inverse of the effective Prandtl number for k and ε; S_k and S_ε are the user defined source term.

In the high Re limit, μ_{eff} is to be governed by μ_t, given as

$$\mu_t = \frac{C_\mu \rho k^2}{\varepsilon} \qquad (6)$$

The additional term R_ε is defined as

$$R_\varepsilon = \frac{C_\mu \rho \eta^3 \left(1 - \eta/\eta_0\right)}{1 + \beta \eta^3} \cdot \frac{\varepsilon^2}{k}, \qquad (7)$$

where, $\eta = S(k/\varepsilon)$, S is the modulus of the mean rate of the strain tensor. The coefficients for RNG $k - \varepsilon$ model are given in Table 1.

Table 1

Coefficients for RNG $k - \varepsilon$ model

$C_{1\varepsilon}$	$C_{2\varepsilon}$	C_μ	η_0	β
1.42	1.68	0.0845	4.38	0.012

As an external flow, the air flow is used, the initial velocity of the air at the channel's entrance region varied $u = 1.33 \div 14$ m/s at a temperature of $56.5°$ C and atmospheric pressure. The temperature of the tube surface is $20.8°$ C. Boundary conditions are shown in Fig. 1 beside the geometry of the numerical model.

The flow characteristics of the staggered tube bundles in cross flow can be represented with the Reynolds number defined by the maximum velocity in the minimum free cross-section and the equivalent diameter as follows:

$$\mathrm{Re}_{D,\max} = \frac{\rho U_{\max} D_{eq}}{\mu} \qquad (8)$$

where, μ is a dynamic viscosity, and $U_{\max}$ is the maximum velocity in the minimum free cross section.

In this study, two air velocities were considered at the entrance to the channel $u = 1.33 \div 14$ m/s, corresponding to Reynolds numbers $\mathrm{Re}_{D,\max} = 3.18 \times 10^3 \div 3.25 \times 10^4$.

2.1. Mesh generation

Figure 4 shows the configuration of the computational domain mesh using ANSYS FLUENT. The working fluid domain is meshed with quad and triangle mesh elements with refining the mesh near walls that ensure $y^+ < 1$. The mesh quality of 0.81 is maintained for the entire simulation.

In this study, a finite-volume discretization method using second-order upwind scheme for momentum, turbulent kinetic energy, and turbulent dissipation rate was performed. The simulation used the segregated solver. Continuity and momentum equations were solved in a decoupled fashion during the outer iteration loop, besides using SIMPLE pressure-based solution algorithm of the velocity–pressure coupling. The solution was considered converged when the scaled residual of the energy and other equations reach 10^{-8}.

The mesh-sensitivity analysis was carried out mainly to check for a mesh independent solution. The number of nodes varied from 13508 to 347766. It is seen from Fig. 5 that the computational Nu_{av} of a drop-shaped tubes bundle becomes independent from the mesh for the mesh of about 225456

nodes for all studied cases of longitudinal spacing. Hence, the mesh of 225456 nodes is considered here-onwards to optimize the time and the accuracy of the solution.
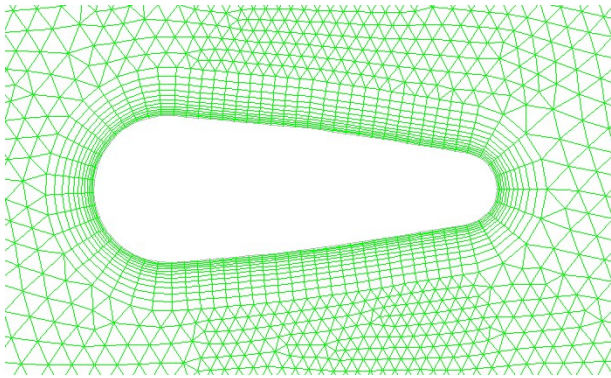

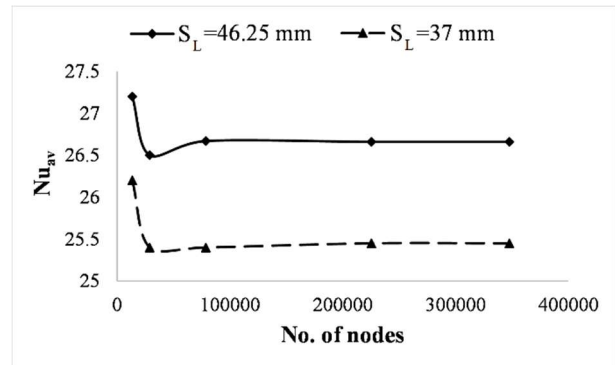Fig. 4. Mesh details around the tube surface

Fig. 5. Mesh-sensitivity analysis at $u = 1.33$ m/s

2.   Discussion of the results obtained

2.1.   Numerical results verification

In order to validate the numerical model, the heat transfer from a single circular tube with an equivalent diameter of 22.5 mm (Fig. 2) is simulated and compared with the results obtained by Zhukauskas [11] in the same range of values of Reynolds numbers. The numerical model and mesh are quite similar to those used in the case of a drop-shaped tube.
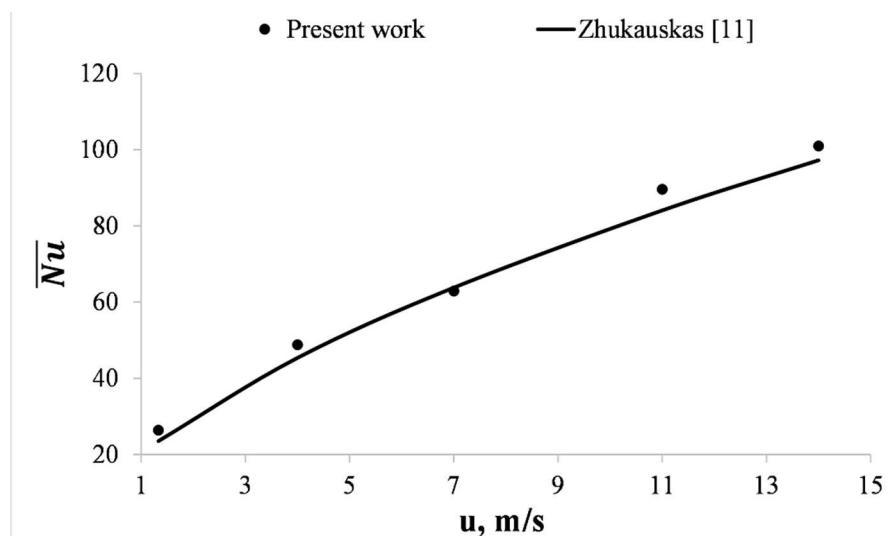

Fig. 6. Validation of Nu versus *u*

As seen from Fig. 6, the results of this study agree well with the results of Zhukauskas, indicating that the model and the method of the CFD simulation presented in this study is reliable.

2.2.   Streamline and velocity contours

The streamline provides the details of the separation point and it indicates the intensity and location of the vortex formation at the tube downstream. For all cases of longitudinal spacing and the air velocity of 1.33 m/s (Fig. 7, *a*; *c*), it is clear that there are three separation zones: two at the lateral and one at the rear surfaces of the tubes. The flow separation occurs as a result of travelling of the boundary layer far enough against an adverse pressure gradient, that makes the velocity of the particles nearest to the surface falls almost to zero.

With increasing the air velocity, the vortices at lateral tube surfaces disappear and the separation occurs only at the rear surface of the tube (Fig. 7, *b*; *d*). This is due to the fact that, for high velocities, the flow becomes more energetic enabling the boundary layer to travel farther along the tube surface before separation. It is observed that the strong vortex decreases as the longitudinal spacing increases from 37 to 46.25 mm.
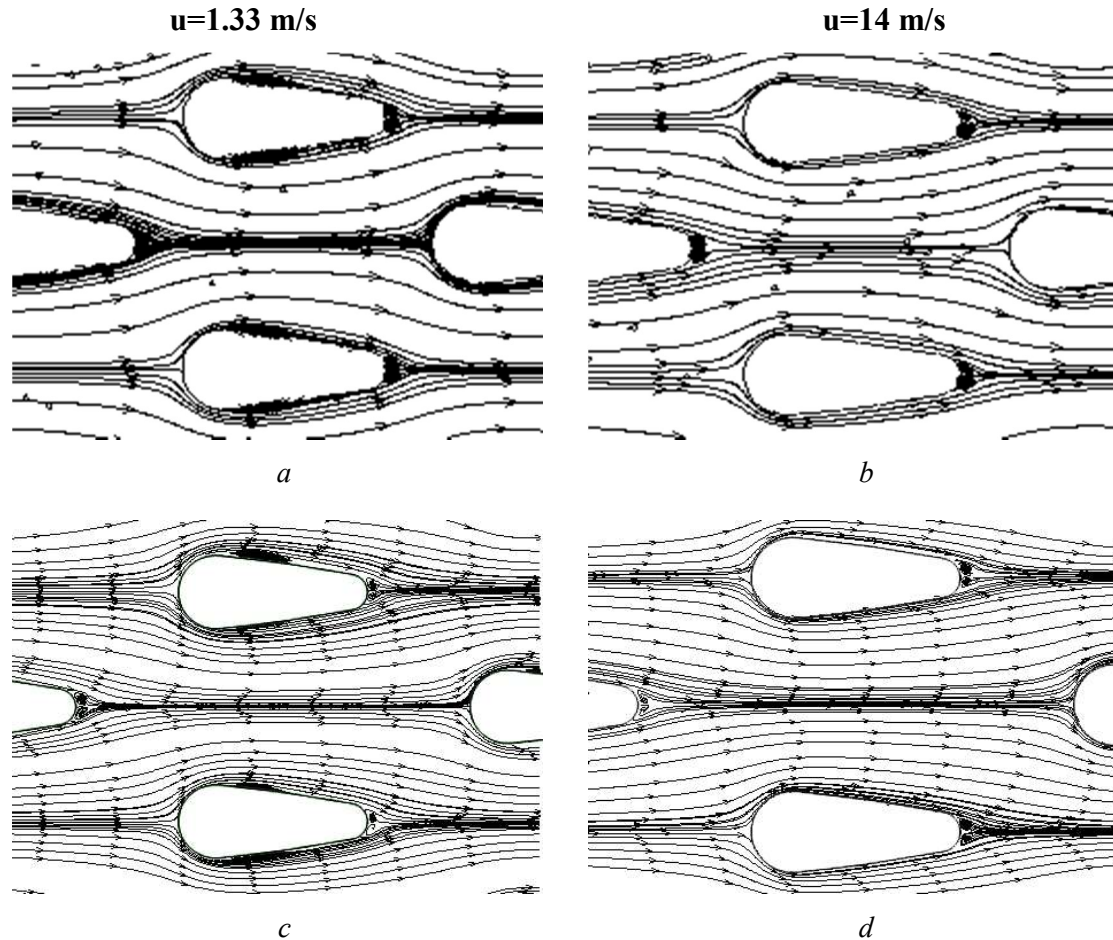
u=1.33 m/s   **u=14 m/s**

a   *b*

c   *d*

Fig. 7. Streamlines of the drop-shaped tubes of the bundle for longitudinal spacing S_L of: 37 mm (*a, b*); 46.25 mm (*c, d*) at $u = 1.33$ and 14 m/s

2.3. Temperature and heat transfer characteristics over the tubes bundle

The temperature of the tube surface increases by gaining the heat from the incoming air. Figure 8 demonstrates the temperature contours of the drop-shaped tubes bundle for two cases of the longitudinal. As the air velocity increases, the turbulence area behind the tubes, in a narrower rear surface of the tubes, gradually increases, which contributes to a further improvement in heat transfer. With increasing the longitudinal spacing, the area of the higher temperature air zone increases (Fig. 8, *c*; *d*).

The heat transfer is affected by the development of the hydrodynamic boundary layer over the surface of the tube. Figure 9 shows the heat transfer coefficient averaged over whole surface of the tubes bundle for the air velocity in ranger of $1.33 \div 14$ m/s. The average Nusselt number increases with the increase in the air velocity and/or the longitudinal spacing for the studied cases. At low air velocities, the difference between the average Nusselt number values for the longitudinal spacing of 37 and 46.25 mm is small. This difference increases with increases in air velocities. This can be attributed to the high turbulence in wakes of downstream tubes which makes the boundary layer of tubes rows thinner.

The average Nusselt number of a bundle was determined from the computational experiment results as

$$\overline{Nu} = \frac{\overline{\alpha}D}{\lambda},\qquad(9)$$

where $\overline{\alpha} = \dfrac{1}{F}\displaystyle\int_0^F \alpha\,dF$ is the heat transfer coefficient averaged over whole surface of tubes bundle. The values of the heat transfer coefficient were obtained from the results of the computational experiment using ANSYS program.
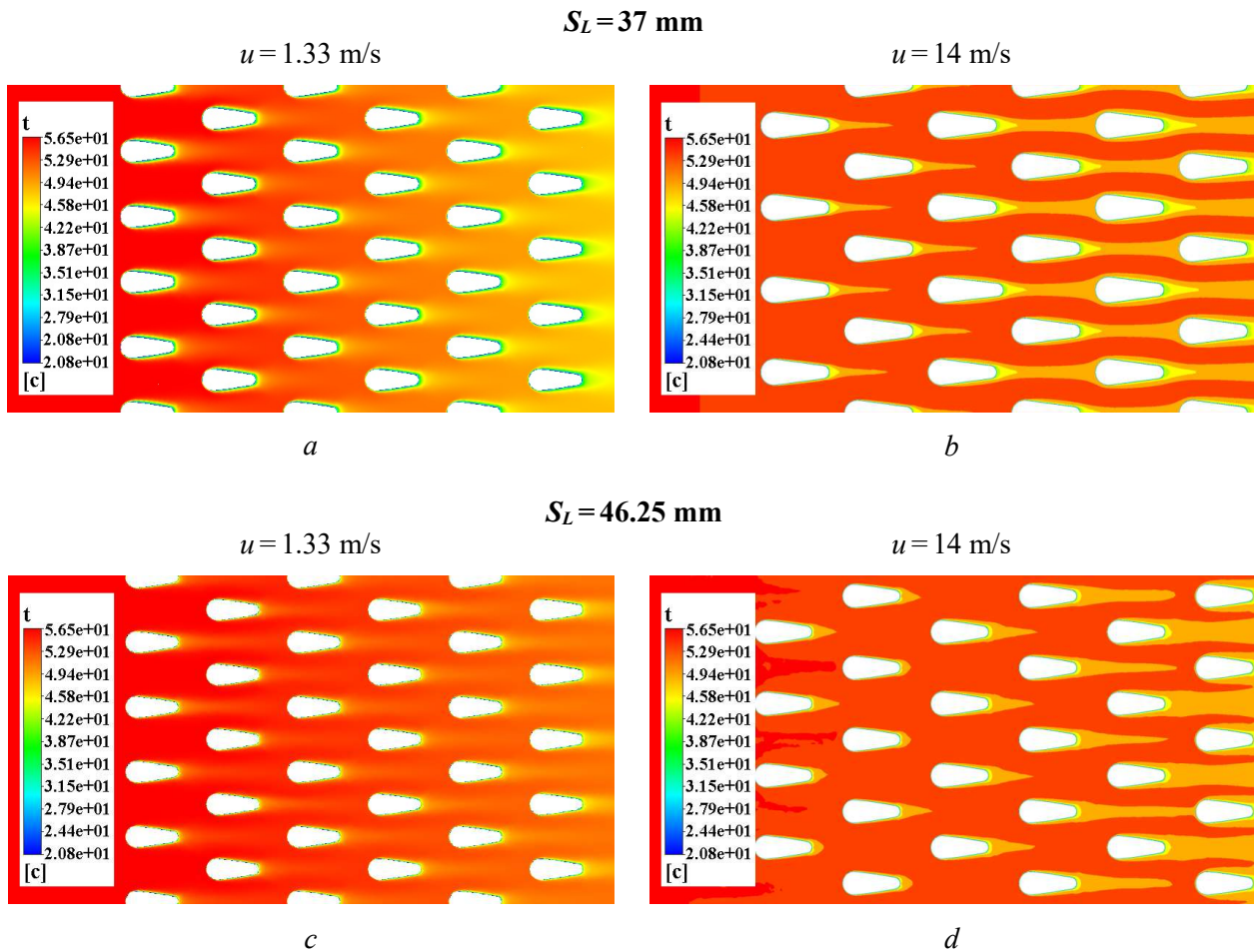
$S_L = 37$ mm

$u = 1.33$ m/s

$u = 14$ m/s

a

b

$S_L = 46.25$ mm

$u = 1.33$ m/s

$u = 14$ m/s

c

d

Fig. 8. Temperature contours for drop-shaped tubes bundle with S_L of 37 mm (*a, b*), and 46.25 mm (*c, d*) at $u = 1.33 \div 14$ m/s
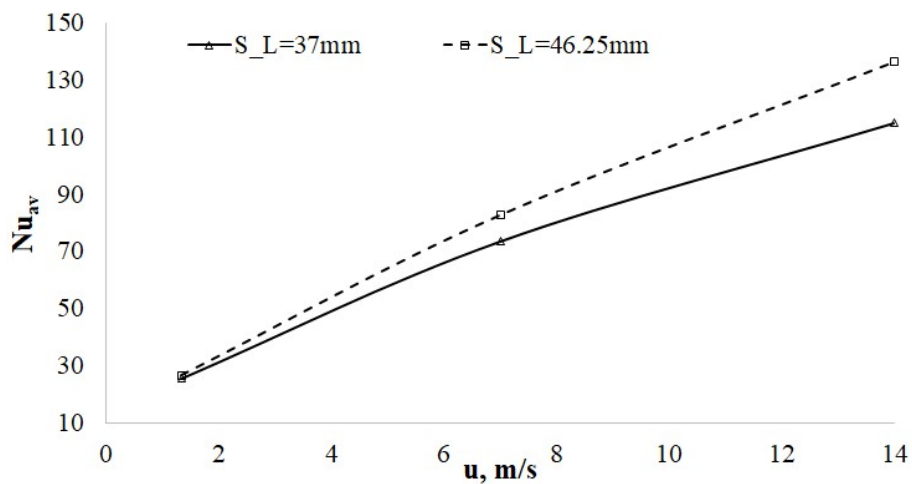

Fig. 9. Average Nusselt number vs air velocity

9

Correlation for the average non-dimensional Nusselt number for the staggered drop-shaped tubes bundle based on the computational experiment obtained for various Reynolds numbers and the longitudinal spacing was predicted by equation (10):

$$\overline{\mathrm{Nu}} = 0.2172.\mathrm{Re}^{0.6442}\,\mathrm{Pr}^{1/3}\left(0.5+\frac{S_L}{0.074}\right)^{-2.7656\times 10^{-3}}, \qquad (10)$$

where the thermo-physical properties [31] are calculated for the average temperature of the incoming flow. The obtained correlation is applicable for $\mathrm{Re}_{D,\max} = 3.18\times 10^3 \div 3.25\times 10^4$ and for $S_L = 37 \div 46.25$ mm. Figure 10 shows a comparison of present correlation with other results from previous studies.
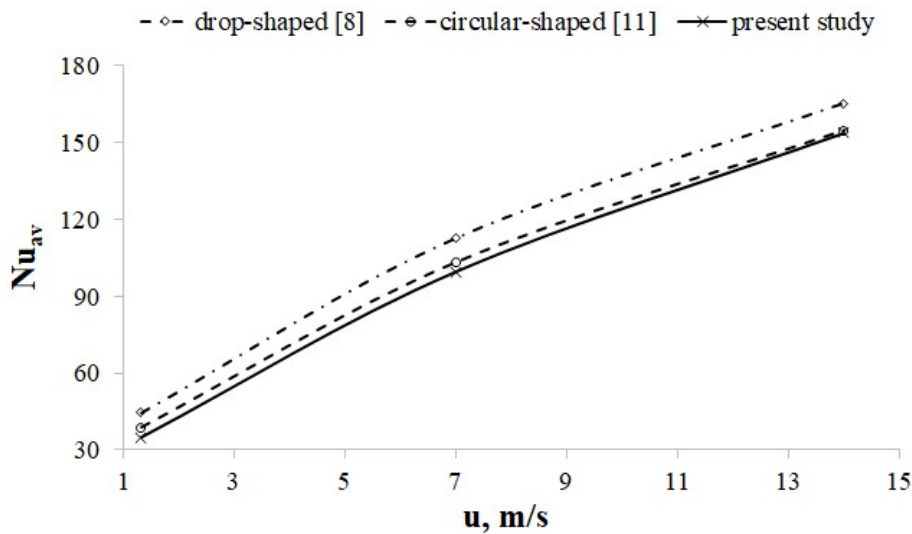

Fig. 10. Comparison of present Nu vs u results with previous works for S_L of 37 mm

It is clear that that there is a slight difference between the values calculated by Eq. (10) and the values calculated by 8] for zero angle of attack, which does not reflect the effect of the longitudinal spacing on the heat transfer. Also, as seen in Fig. 10, circular tubes [11] are better in terms of heat transfer compared to drop-shaped tubes, this can be attributed to the large turbulence area behind the circular tubes, which contributes to improving the heat transfer.

2.4. Friction factor

Figure 11 shows the distribution of the pressure for drop-shaped tubes bundles for two cases of the longitudinal spacing and the air velocity. For all studied cases, it is clear that the pressure has the highest value at the stagnation point on the front of the tube, this is due to the fact that the flow velocity at this point tends to zero (Fig. 13). When the flow passes over the surface of the tube, the pressure decreases to the lowest value on the lateral surface.

Friction factor f is defined as

$$f = \frac{\Delta P}{0.5\rho U_{\max}^2 N_L}, \qquad (11)$$

where ΔP is pressure drop across the bundle (from the simulation results); N_L is number of transverse rows.

Figure 12 indicates the friction factor for drop-shaped tubes bundles. The friction factor for the fluid decreases, with an increase in the air velocity. This is usually due to the fact that the overall drag consists of two combined parts: the friction drag, and the pressure drag.
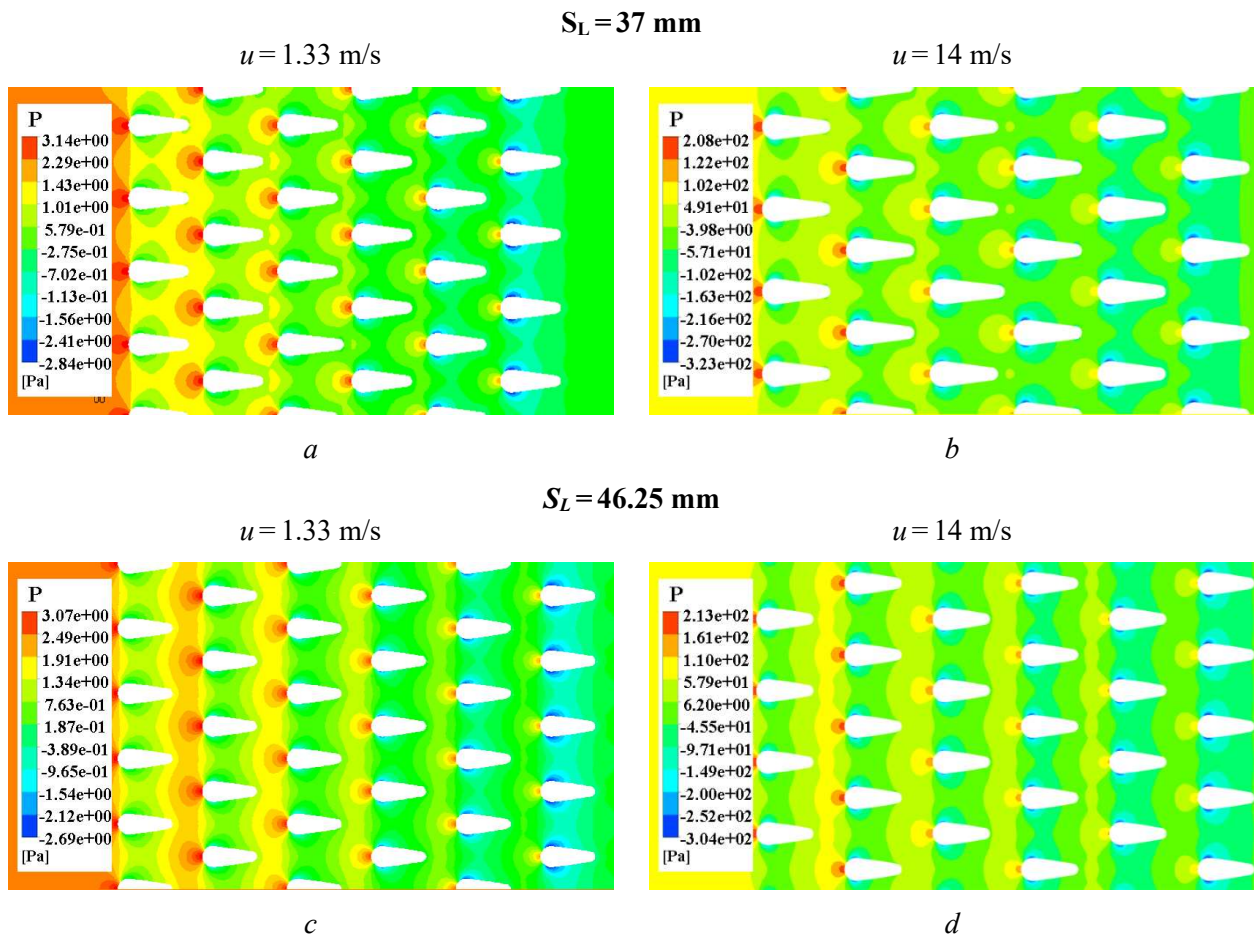
S$_L$ = 37 mm

u = 1.33 m/s u = 14 m/s

a   b

S$_L$ = 46.25 mm

u = 1.33 m/s u = 14 m/s

c   d

Fig. 11. Pressure contours for drop-shaped tubes bundle with S_L of 37 mm (*a*, *b*), and 46.25 mm (*c*, *d*) at u = 1.33 ÷ 14 m/s
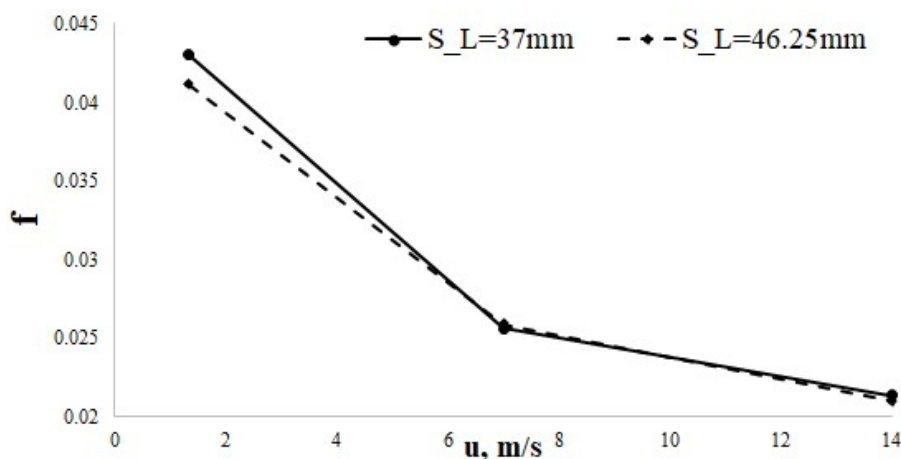

Fig. 12. Friction factor vs air velocity for drop-shaped tubes bundle for S_L of 37 mm and 46.25 mm

The friction drag is more dominant than the pressure drag at the lower velocities, which results in a higher pressure drop while the opposite occurs at the higher velocities. In the case of high velocities, the influence of viscous forces decreases while that of the inertial forces increases. Since the airflow tends to shift more turbulent, the separation point travels farther downstream, and consequently the size of the wake and the magnitude of the pressure drag decreases. The maximum value of the friction factor for drop-shaped tubes with S_L of 37 and 46.25 mm is found to be 0.43 and 0.41, respectively.
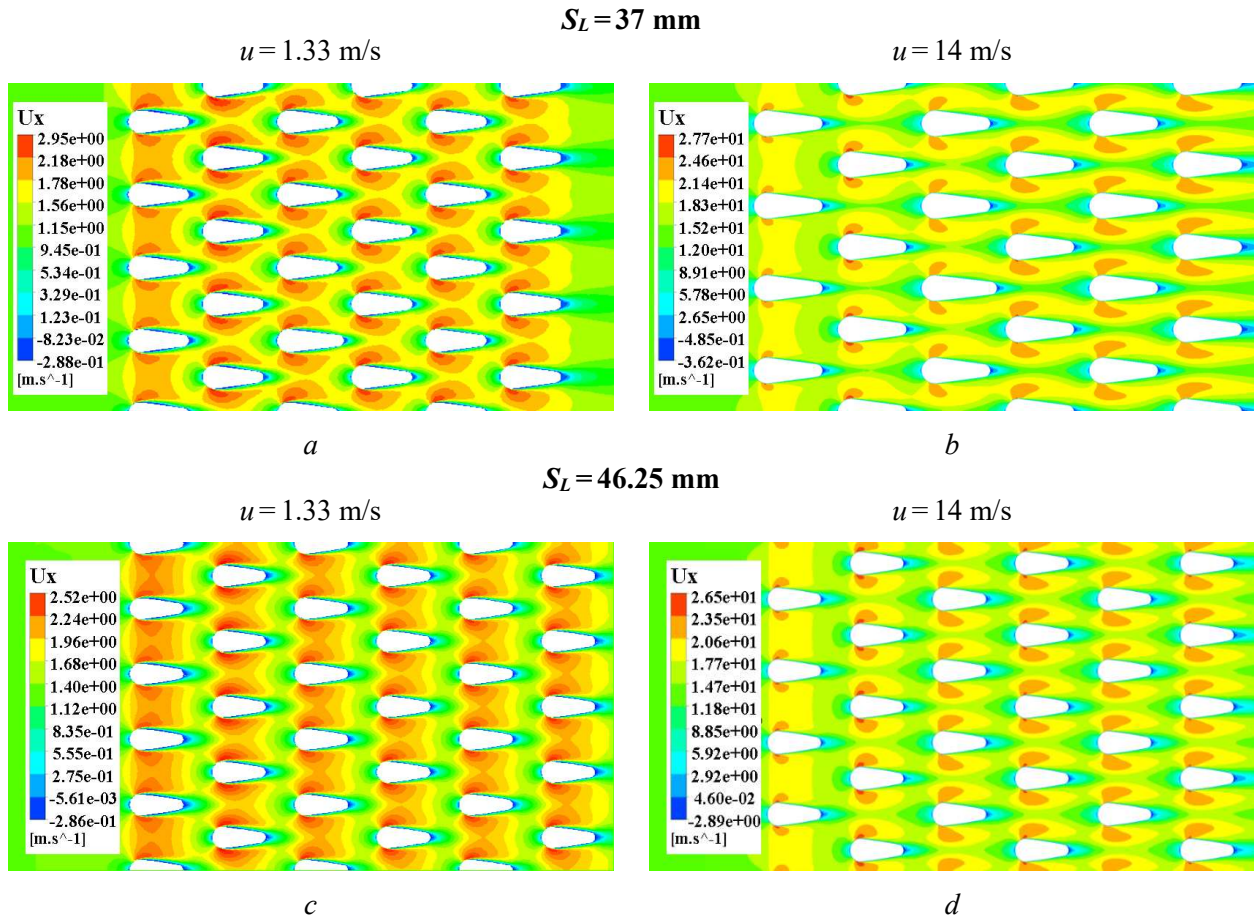
11

$S_L = 37$ mm

$u = 1.33$ m/s $u = 14$ m/s

a   b

$S_L = 46.25$ mm

$u = 1.33$ m/s $u = 14$ m/s

c   d

Fig. 13. Velocity contours for drop-shaped tubes bundle with S_L of 37 mm (*a*, *b*), and 46.25 mm (*c*, *d*) at $u = 1.33 \div 14$ m/s

The friction factor data can be correlated using a dimensionless relation of the form

$$f = 0.4592 \cdot \mathrm{Re}^{-0.29631} \qquad (12)$$

The obtained correlation can be used for $\mathrm{Re}_{D,\max} = 3.18 \times 10^3 \div 3.25 \times 10^4$ and for $S_L = 37 \div 46.25$.

2.5. Thermal-hydraulic performance

The above sections have discussed the heat transfer characteristics and the friction factor for the bundle of the drop-shaped tubes. However, it is necessary to evaluate the combined effect of heat transfer along with friction factor associated with the flow over the tubes bundle. The thermal-hydraulic performance for the entire range of the air velocity is depicted in Fig. 14.

The thermal hydraulic performance of drop-shaped tube heat exchanger is proposed by Webb [32] as

$$\eta = \frac{\overline{\mathrm{Nu}}_{av,drop-shaped} / \overline{\mathrm{Nu}}_{av,circular-shaped}}{f_{drop-shaped} / f_{circular-shaped}} \qquad (13)$$

For drop-shaped tubes, it is clear from Fig. 14, that the thermal–hydraulic performance increases as air velocity increases. A tubes bundle with a longitudinal spacing of 46.25 mm is much superior to a longitudinal spacing of 37 mm. On the other hand, a drop-shaped tubes bundle with $S_L = 46.25$ mm has more intense heat transfer with less hydrodynamic resistance as compared to that

with $S_L = 37$ mm. Also, it is clear that the thermal–hydraulic performance of drop-shaped tube bundle with staggered arrangement is about $18.1 \div 43.7$ times greater than circular tube bundle. As a result, the drop-shaped tube bundle performs better than a circular one. This can be attributed to its aerodynamic shape and lower friction factor compare to a circular tube.
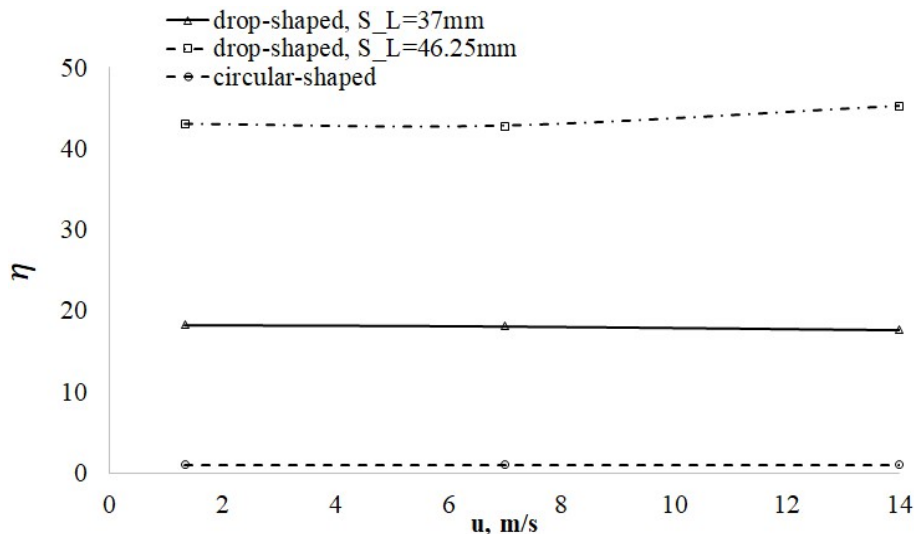

Fig. 14. Thermal–hydraulic performance of drop-shaped tube bundle and circular tube bundle

3.   Conclusion

The heat transfer and fluid flow behavior in the case of a staggered drop-shaped tubes bundle have been studied numerically. The study is performed for the Reynolds number range from 3.18×10^3 to 3.25×10^4, while the longitudinal spacing is 37 and 46.25 mm. Some of the key aspects of this study are as follows:

1.   A mathematical model and calculation algorithm have been developed to calculate the heat transfer and friction factor of staggered double drop-shaped tubes bundle using the ANSYS package, with taking into account the stress-strain state of the tubes.
2.   The average Nusselt number increases with the increase in the air velocity and/or the longitudinal spacing for the studied cases.
3.   Amongst two longitudinal spacing of 37 and 46.25 mm, a bundle with a longitudinal spacing of 46.25 mm, has the maximum thermal–hydraulic performance.
4.   Correlations were developed from the computational experiment results for the bundle of drop-shaped tubes to give the average Nusselt number and friction factor in terms of Re and S_L.
5.   As the air velocity increases, the friction factor decreases.
6.   The drop-shaped tubes provide the better thermal–hydraulic performance, as compared to that of the circular tubes.

The results obtained will serve as a base for further studies of the heat transfer and hydrodynamic characteristics of drop-shaped tubes bundle.

References

1.   Zhang, L. W., Balachandar, S., Tafti, D. K., Najjar, F. M., "Heat transfer enhancement mechanisms in inline and staggered parallel-plate fin heat exchangers," *International Journal of Heat and Mass Transfer*, Vol. 40, 1997, pp. 2307–2325.
2.   Chen, Y., Fiebig, M., Mitra, N. K., "Heat transfer enhancement of finned oval tubes with staggered punched longitudinal vortex generators," *International Journal of Heat and Mass Transfer*, Vol. 43, 2000, pp. 417–435.

3.   Nishimura, T., Hisayoshi, I., Hisashi, M., "The influence of tube layout on flow and mass transfer characteristics in tube banks in the transitional flow regime," *International Journal of Heat and Mass Transfer*, Vol. 36, No. 3, 1993, pp. 553−563.

4.   Lavasani, A. M., Bayat, H., Maarefdoost, T., "Experimental study of convective heat transfer from in-line cam shaped tube bank in crossflow," *Applied thermal engineering*, Vol. 65, No. 1-2, 2016, pp. 85−93.

5.   Toolthaisong, S., and Kasayapanand, N., "Effect of attack angles on air side thermal and pressure drop of the cross-flow heat exchangers with staggered tube arrangement," *Energy Procedia*, Vol. 34, 2013, pp. 417–429.

6.   Merker, G. P., Hanke, H., "Heat transfer and pressure drop on the shell-side of tube-banks having oval-shaped tubes," *International Journal of Heat and Mass Transfer*, Vol. 1299, No. 12, 1986, pp. 1903−1909.

7.   Horvat, A., Leskovar, M., Mavko, B., "Comparison of heat transfer conditions in tube bundle cross-flow for different tube shapes," *International Journal of Heat and Mass Transfer*, Vol. 49, 2006, pp. 1027–1038.

8.   Sayed, E. A. S. A., Emad, Z. I., Osama, M. M., Mohamed, A. A., "Heat transfer characteristics of staggered wing-shaped tubes bundle at different angles of attack," *Heat and Mass Transfer*, Vol. 50, No 8, 2014, pp. 1091–1102.

9.   Sayed, E. A. S. A., Emad, Z. I., Osama, M. M., Mohamed, A. A., "Effect of attack and cone angels on air flow characteristics for staggered wing shaped tubes bundle," *Heat and Mass Transfer*, Vol. 51, No. 7, 2014, pp. 1001–1016.

10.   Zhukauskas, A., Ulinskas, R. V., "Efficiency parameters of heat transfer in tube banks," *Heat Transf Eng*. Vol. 6, No. 1, 1985, pp. 19–25.

11.   Zhukauskas, A., "Heat transfer from tubes in cross-flow," *Advance Heat Transfer*, Vol. 8, 1972, pp. 93−160.

12.   Chilton, T. H., Generaux, R. P., "Pressure Drops Across Banks of Tubes," *AIChE Transactions*, Vol. 29, 1933, pp. 161−173.

13.   Grimison, E. D., "Correlation and utilization of new data on flow resistance and heat transfer for cross flow of gases over tube banks," *Transactions ASME*, Vol. 59, 1937, pp. 583–594.

14.   Huge, E. C., "Experimental investigation of effects of equipment size on convection heat transfer and flow resistance in cross flow of gases over tube banks," *Transactions ASME*, Vol. 59, 1937, pp. 573–581.

15.   Pierson, O. L., "Experimental investigation of the influence of tube arrangement on convection heat transfer and flow resistance in cross flow of gases over tube banks," *Transactions ASME*, Vol. 59, 1937, pp. 563–572.

16.   Gunter, A. Y., Shaw, W. A., "A General Correlation of Friction Factors of Various Types of Surfaces in Cross Flow," *Transactions ASME*, Vol. 67, 1945, pp. 643−660.

17.   Kim, T., "Effect of longitudinal spacing on convective heat transfer in crossflow over in-line tube banks," *Annals of Nuclear Energy*, Vol. 57, 2013, pp. 209–215.

18.   Mittal, S., Kumar, V., Raghuvanshi, A., "Unsteady incompressible flows past two cylinders in tandem and staggered arrangements," *Int. Journal for Numerical Methods in Fluids*, Vol. 25, No. 11, 1997, pp. 1315−1344.

19.   Roychowdhury, G. D., Sarit, K. D., Sundararajan, T., "Numerical simulation of laminar flow and heat transfer over banks of staggered cylinders," *International Journal of Numerical Methods in Fluids*, Vol. 39, 2002, pp. 23−40.

20.   Nishiyama, H., Ota, T., Matsuno, T., "Heat transfer and flow around elliptic cylinders in tandem arrangement," *JASME Int. J. Ser II*, Vol. 31, No. 3, 1988, pp. 410–419.

21. Mahir, N., Altac, Z., "Numerical investigation of convective heat transfer in unsteady flow past two cylinders in tandem arrangements," *Int. Journal of Heat and Fluid Flow*, Vol. 29, No. 5, 2008, pp. 1309−1318.

22. Deng, J., Ren A., FengZou, J., Shao, X., "Three-dimensional flow around two circular cylinders in tandem arrangement," *Fluid Dyn. Res.*, Vol. 38, 2006, pp. 386−404.

23. Zdravistch, F., Fletcher, C., Behnia, M., "Numerical laminar and turbulent fluid flow and heat transfer predictions in tube banks," *Int. J. Numer. Methods Heat Fluid Flow*, Vol. 5, No. 8, 1995, pp. 717−733.

24. Robertson, E., Chitta, V., Walters, D. K., Bhushan, S., "On the vortex breakdown phenomenon in high angle of attack flows over delta wing geometries," *International Mechanical Engineering Congress & Exposition, IMECE2014*, Montreal, Canada, November 14–20, 2014.

25. Jafari, H. H., Dehkordi, B. G., "Numerical prediction of fluid-elastic instability in normal triangular tube bundles with multiple flexible circular cylinders," *J. of Fluids Engineering*, Vol. 23, No. 1, 2011, pp.114−126.

26. Priyank, D. P., Karnav, N. S., Kush, V. M., Chetan, O. Y., "CFD analysis of heat exchanger over a staggered tube bank for different angle arrangement of tube bundles," *International Journal of Engineering Research and Technology*, Vol. 2, No. 1, 2013, p. 2278-0181.

27. Yakhot, V. et al., "Renormalization Group Modeling and Turbulence Simulations," International Conference on Near-Wall Turbulent Flows. Arizona. Tempe. 1993.

28. Frank, K., Raj, M. M., Mark, S. B., *Principles of heat transfer*, Stamford. CT Singapore: Cengage Learning. 2011.

29. Soe, T. M., Khaing, S. Y., "Comparison of turbulence models for computational fluid dynamics simulation of wind flow on cluster of buildings in Mandalay," *International Journal of Scientific and Research Publications*, Vol. 7, No. 8, 2017, pp. 2250−3153.

30. ANSYS Fluent Reference Guide. ANSYS. Inc. Release 16.0. 2015.

31. Tsvetkov, F. F., *Zadachnik po teplomassoobmenu* (Problem book in heat and mass transfer), F.F. Tsvetkov, R.V. Kerimov, V.I. Velichko. Moscow, MEI Publ, 2008, 196 p., ill. (in Russian).

32. Webb, R. L., "Performance evaluation criteria for use of enhanced heat transfer surfaces in heat exchanger design," *International Journal of Heat and Mass Transfer*, Vol. 24, 1981, pp. 715−726.